A micromachined dual-band orthomode transducer

Leal-sevillano, Carlos A.; Tian, Yingtao; Lancaster, Michael J.; Ruiz-cruz, Jorge A.; Montejo-garai, Jose R.; Rebollar, Jesus M.

DOI:
10.1109/TMTT.2013.2292611

A Micromachined Dual-Band Orthomode Transducer

Carlos A. Leal-Sevillano, *Student Member, IEEE*, Yingtao Tian, Michael J. Lancaster, *Senior Member, IEEE*, Jorge A. Ruiz-Cruz, *Senior Member, IEEE*, José R. Montejo-Garai, and Jesús M. Rebollar

***Abstract*—In this paper, an orthomode transducer (OMT) for dual-band operation and optimized for stacked micromachined layers implementation is presented. The proposed design avoids the use of septums, irises, pins, or small features and minimizes the number of equal-thickness micromachined layers required. In this way, the micromachining fabrication is simplified, making the proposed design a very attractive candidate for high frequency applications and for low-cost batch production. A W-band dual-band design (one different polarization in each frequency band) with more than 10% fractional bandwidth for each band and 30% separation between bands is presented. In addition, proper routing and layered bends are designed for an optimum standard interfacing with the same orientation of the input/output ports. Two OMTs in a back-to-back configuration are fabricated using a thick SU-8 photo-resist micromachining process. A total of six stacked SU-8 layers, all of them with the same thickness of 635 μm, are used. The experimental results are coherent with the tolerance and misalignment of the process, validating the proposed novel OMT design.**

***Index Terms*—Dual-band, micromachining, orthomode transducer (OMT), SU-8, W-band, waveguide.**

I. Introduction

ORTHOMODE transducers (OMTs) are passive devices with three physical ports that can be represented as a four-port electrical network: the fundamental mode at the lateral and axial ports and two polarizations (vertical and horizontal) at the common port [1]. These polarizations are the two fundamental modes propagating at the common port. Following the nomenclature defined in Fig. 1, it is ideally intended total transmission between vertical polarization and axial port and between horizontal polarization and lateral port. In that sense, an OMT can be seen as a 0-dB dual-polarization directional coupler.

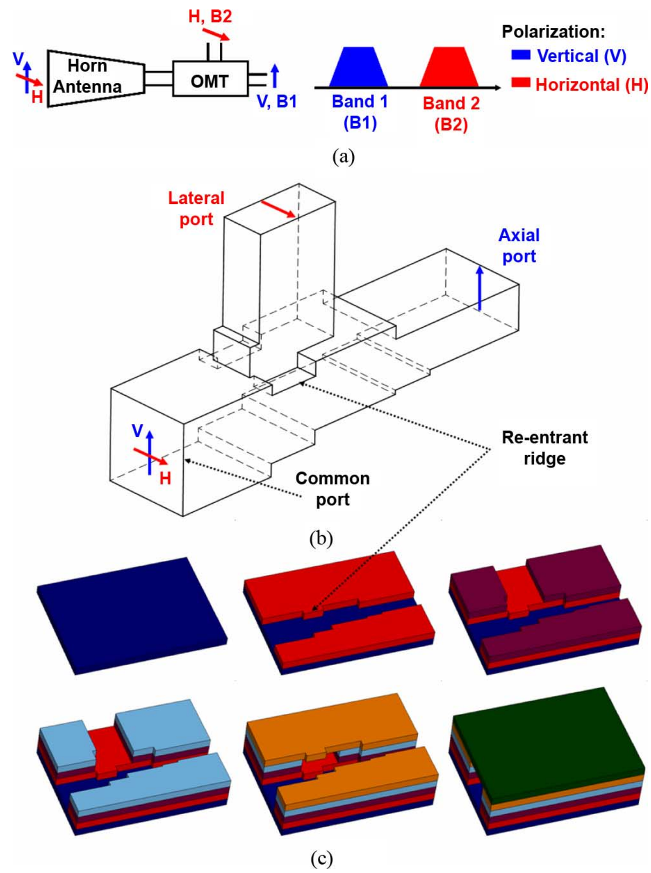

Fig. 1. (a) Operation of the dual-band single polarization OMT. (b) Proposed OMT for optimum implementation with staked micromachined metal layers. (c) Schematic of the six equal-thickness layers.

These kinds of devices are used in the front-ends of numerous high-frequency transceivers to significantly improve and enhance their electrical capabilities. They allow the operation with both orthogonal linear polarization using a single horn and a single reflector antenna, with the subsequent volume and mass savings. This unique property makes OMTs essential elements in widespread applications covering terrestrial and space communications, satellite on-board equipment, radio-astronomy systems, and scientific instrumentation.

There exist different waveguide junctions used as OMTs, which can be classified into different categories [2]. These waveguide junctions can be gathered into two main groups: with onefold or with twofold symmetry. This classification is convenient in order to establish the maximum achievable bandwidth being set by the excitation of higher order modes. In the case with onefold symmetry, the main OMT structures

Manuscript received May 29, 2013; revised November 18, 2013; accepted November 19, 2013. Date of publication December 05, 2013; date of current version January 06, 2014. This work was supported by the U.K. Engineering and Physical Science Research Council, the Spanish Government Program TEC2010-17795, the CONSOLIDER CSD2008-00068, and the Universidad Politécnica de Madrid under a Ph.D. grant.

C. A. Leal-Sevillano is with the Departamento de Electromagnetismo y Teoría de Circuitos, ETSI Telecomunicación, Universidad Politécnica de Madrid, Madrid 28040, Spain and also with the Escuela Politécnica Superior, Universidad Autónoma de Madrid, Madrid 28049, Spain (e-mail: caleal@etc.upm.es).

Y. Tian and M. J. Lancaster are with the School of Electronics, Electrical and Computer Engineering, The University of Birmingham, Edgbaston, Birmingham B15 2TT, U.K. (e-mail: y.tian@bham.ac.uk; m.j.lancaster@bham.ac.uk).

J. A. Ruiz-Cruz is with the Escuela Politécnica Superior, Universidad Autónoma de Madrid, Madrid 28049, Spain (e-mail: Jorge.RuizCruz@uam.es).

J. R. Montejo-Garai and J. M. Rebollar are with the Departamento de Electromagnetismo y Teoría de Circuitos, ETSI Telecomunicación, Universidad Politécnica de Madrid, Madrid 28040, Spain (e-mail: jr@etc.upm.es; jmrm@etc.upm.es).

Color versions of one or more of the figures in this paper are available online at http://ieeexplore.ieee.org.

Digital Object Identifier 10.1109/TMTT.2013.2292611

are based on T-junctions. In these T-junctions, either the horizontal [3]–[6] or the vertical [7], [8] polarization can be guided through the lateral port. Another different approach is based on backward coupling structures [9]. In addition, stringent specifications for single or multiple frequency bands and with one or both polarizations per band are commonly desired [7].

The fabrication of OMTs is normally carried out by using accurate machining processes, such as CNC milling, electric discharge (EDM), or electroforming. However, these techniques are rather expensive and particularly cumbersome when going to millimeter and submillimeter-wave bands. Moreover, they are in general not adequate for mass production of high-frequency devices, which is one of the goals for new-generation array-based instruments [10].

As alternatives to metal machining processes, new emerging micromachining techniques [11] have been proposed recently. Some of these technologies are SU-8 [12]–[14], DRIE [15], [16], or LIGA [17], and all of them are of special interest for high-frequency waveguide components. These technologies have in common that they are produced from different metallized layers that are stacked to assemble the final component. These micromachining processes have been applied for the implementation of different passive waveguide devices including filters [14], [17], [18], couplers [19], and antennas [11], [20].

In order to properly guide each of the polarizations to a different port, polarization-sensitive elements should be introduced in the OMT junction. Some polarization-sensitive elements are thin septums, pins, and matching thin irises. Unfortunately, these elements cannot be easily implemented by micromachining techniques based on stacked metallized layers. In contrast with the well-know OMT structures with a septum and an iris used for dual- and single-band [3], [4] circuits, we propose a new topology suitable for optimum implementation using micromachining techniques and taking into account its constraints.

II. Novel OMT Structure

In this case, we focus on OMTs capable of performing as dual-band and with a single polarization in each band. These kinds of electrical specifications are common in microwaves for communication equipment, although they could also be used in radio-astronomy and space exploration instruments for the observation of physical phenomena at different frequencies. The desired electrical specifications are summarized as follows:

(a) dual-band single polarization operation;
(b) center frequencies separation 30%;
(c) bandwidth of both bands larger than 10%;
(d) square waveguide at the common port;
(e) standard rectangular waveguides at axial and lateral ports.

In Table I, the particular specifications for the W-band design treated in the following section are shown.

Besides these electrical specifications, several geometric constraints are imposed with the aim of an optimum implementation with micromachined stacked metallized layers:

(1) minimum number of layers;
(2) same thickness of all the stacked layers;

TABLE I
Specifications of the Designed OMT in W-Band (75–110 GHz)

	Band 1	Band 2
Frequency	75-82 GHz	95-105 GHz
Return Loss	> 25 dB	> 25 dB
Isolation	> 50 dB	
XP	> 50 dB	
Interface	WR-10 (2.54 x 1.27 mm)	WR-10 (2.54 x 1.27 mm)
Common port	Square Waveguide (2.54 x 2.54 mm)	

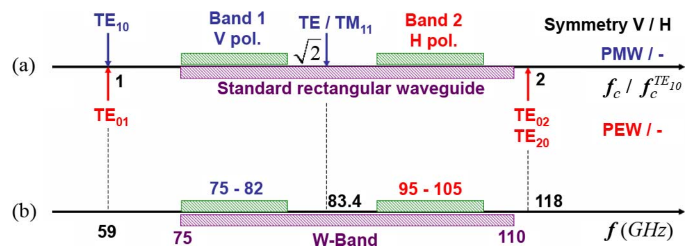

Fig. 2. (a) Mode chart of the square waveguide divided by symmetry. The two operating bands and the optimum standard rectangular waveguide band are highlighted. (b) Dual-band single polarization OMT design at W-band. Side of the square waveguide equal to the standard WR-10 width, 2.54 mm.

(3) avoid the use of septums, posts, or pins;
(4) avoid the use of small features, such as irises or thin waveguide sections.

These geometrical requirements are very restrictive making it challenging to achieve the aforementioned high-performance electrical specifications. Restrictions 1 and 2 simplify the process and speed up the fabrication time. With these constraints, the number of required wafers is minimized and the whole process can be adjusted only for one single etch depth. Restriction 3 is of great importance for actual micromachining processes. Septums and pins would require the fabrication of separate pieces. To this end, specific fabrication techniques should be developed. Moreover, a proper alignment of these separate pieces into the OMT junction would be required. The fourth restriction guarantees a low aspect ratio. In that way, possible fabrication issues are minimized.

One important contribution of this paper is the novel OMT geometry taking into account both the electrical specifications and the geometric constraints. For dual-band single polarization operation [electrical specification (a)], it is well known that OMTs with one symmetry plane can be used [3]. The selection of the rectangular waveguide port for each frequency band depends on the excitation of the $\mathrm{TE}/\mathrm{TM}_{11}$ higher order modes. The rectangular waveguide port, which imposes a perfect electric wall (PEW) at the symmetry plane of the OMT, should be selected for the higher frequency band. This symmetry does not generate the $\mathrm{TE}/\mathrm{TM}_{11}$ modes ensuring a single mode propagation at the common port. The remaining rectangular port should be used for the lower frequency band. The side of the square waveguide at the common port must be small enough to not propagate the $\mathrm{TE}/\mathrm{TM}_{11}$ mode at the lower frequency band. This is illustrated with the mode charts in Fig. 2.

The complete bandwidth, including both bands, is less than 40% [electrical requirements (b) and (c)]. In that way, the same

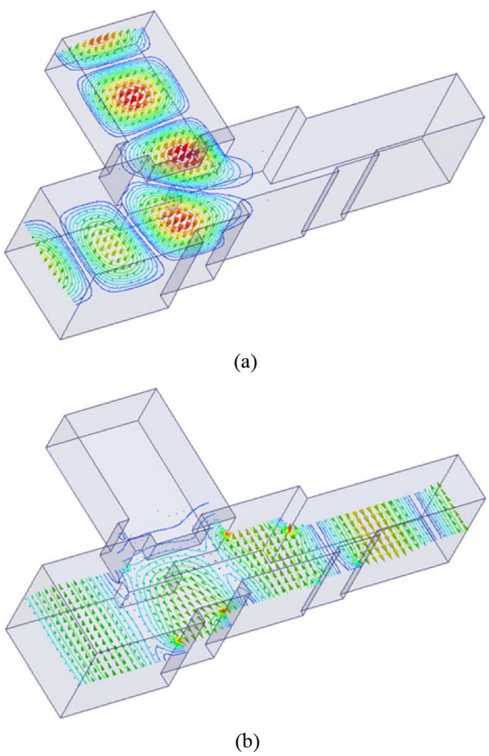

Fig. 3. Electric field for both polarizations. (a) Horizontal polarization at 100 GHz. (b) Vertical polarization at 80 GHz.

standard rectangular waveguide can be used for both bands. This helps restriction 1 since different rectangular waveguides at axial and lateral port would require additional layers. Using the appropriate standard rectangular waveguide, the lower frequency band is close to the lower limit of the standard rectangular waveguide bandwidth. Choosing the side of the square waveguide equal to the width of the standard rectangular waveguide places the cutoff frequency of the $\mathrm{TE}/\mathrm{TM}_{11}$ close to the center frequency of the standard rectangular waveguide and between the two bands of the OMT. Moreover, with this choice of the side of the square waveguide, the number of required layer is minimized, restriction 1.

The last critical point of the OMT is the extraction of the horizontal polarization through the lateral port at the same time that conditions 3 and 4 are fulfilled. This is solved by using a re-entrant ridge at the OMT junction, as shown in Fig. 1(b). This re-entrant ridge helps to guide the electromagnetic beam with horizontal polarization toward the lateral port. This is similar to the approach based on the T-shaped waveguide presented in [8]. Nevertheless, in this case we extract the horizontal instead of the vertical polarization through the lateral port. In Fig. 3, the electric field for each polarization is illustrated. In order to ensure restrictions 1 and 2, only steps on the narrow wall of the rectangular waveguide at the lateral port are introduced [see Fig. 1(b)]. The vertical polarization can be matched by adding waveguide steps at the axial port. These steps do not increase the number of required layers. The final proposed OMT structure with all the geometrical constraints is shown in Fig. 1.

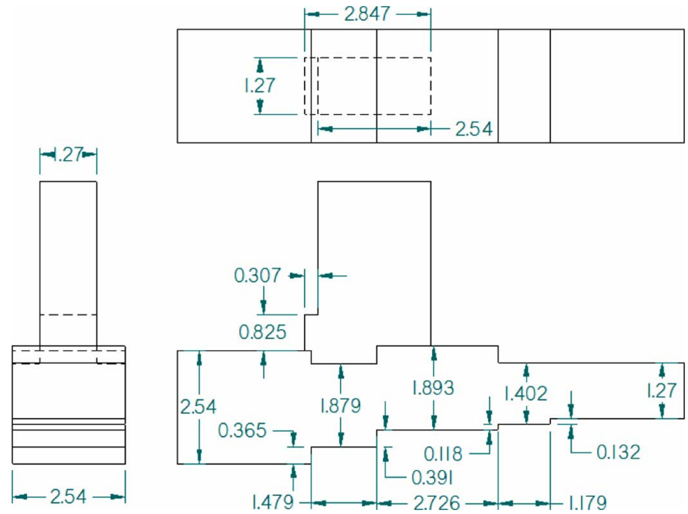

Fig. 4. Final dimensions in millimeters of the W-band OMT design. Front, lateral, and top views of Fig. 1(b).

III. OMT Design

A. OMT Junction Design

Using the geometry proposed in the last section, an OMT with the specifications of Table I is designed. The axial port is matched by using a waveguide transformer from square to rectangular waveguide in a similar way that is presented in [1] and [3]. In this case, four different waveguide sections were required, as depicted in Fig. 4. In principle, the bandwidth for the vertical polarization can be enhanced by using more waveguide sections in the transformer without complicating the final fabrication of the device. At the lateral port, the re-entrant ridge dimensions are adjusted to match the horizontal polarization in the desired frequency band. Moreover, an additional waveguide step is included after the junction to improve the matching of the lateral port, as shown in Fig. 4.

The full-wave simulations were carried out using CST Microwave Studio. The OMT is efficiently analyzed taking advantage of its symmetry. In that way, the full-wave analysis of the OMT is reduced to solve two different problems, which are: 1) the OMT with a perfect magnetic wall (PMW) at the symmetry plane in the lower frequency band and 2) the OMT with a PEW at the symmetry plane in the upper frequency band. In order to get accurate results, a different adaptative meshing at the desired frequency band is used for each subproblem.

The OMT symmetry helps not only in the full-wave analysis, but also to fulfill isolation and cross-polarization isolation specifications. Vertical and horizontal polarizations are isolated due to the onefold symmetry of the OMT's geometry. In that way, the design can be simplified to simultaneously match both polarizations. Isolation and cross-polarization do not need to be optimized since they are infinite due to the symmetry.

The full-wave optimization was carried out using an iterative process based on the efficient algorithms of simplex and simulated annealing [21]. The latter is used in the first iterations of the optimization in order to avoid undesired local minima of the

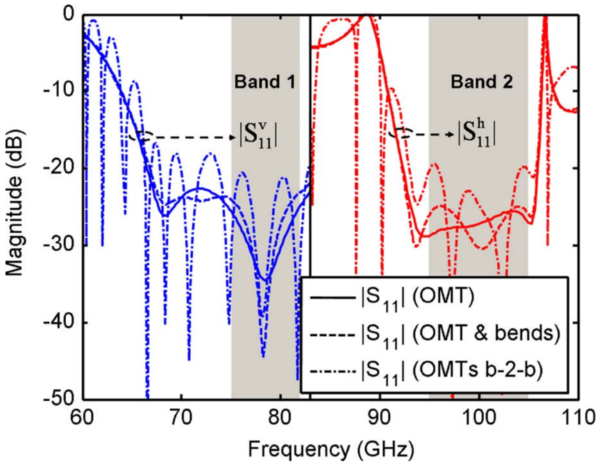

Fig. 5. Full-wave simulations of the dual-band OMT including the OMT, the OMT with bends, and the two OMTs in back-to-back (b-2-b) configuration.

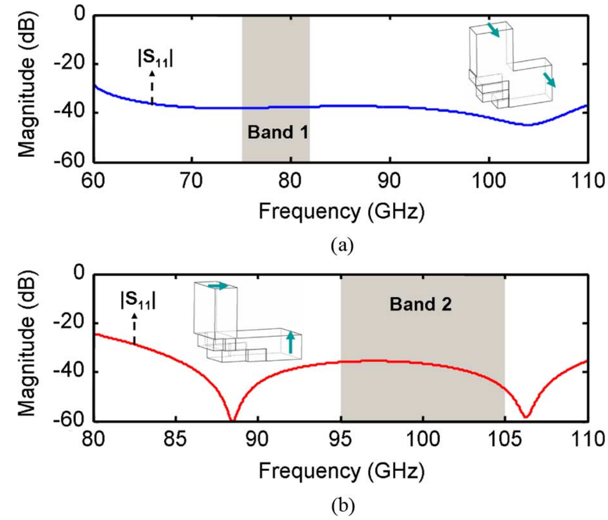

Fig. 6. Full-wave response of the layered 90° bends used at the input/output interfaces. (a) 90° bend in the H-plane. (b) 90° bend in the E-plane.

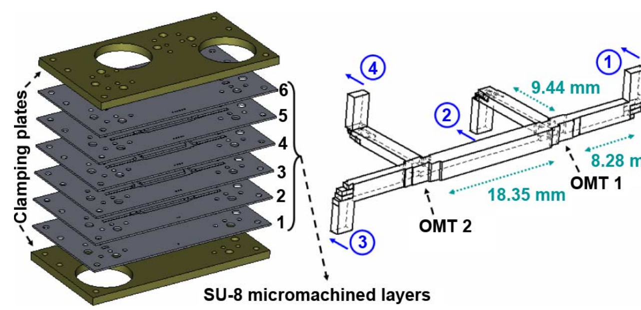

Fig. 7. Final assembly of the OMTs in back-to-back configuration. A total of six metallized SU-8 layers, all of them with 635-μm thickness, in between two metal clamping plates.

error function. The error function to minimize was defined by the nonlinear function

$$F_e = \sum_{i=1}^{N} \left(\Gamma_v\left(f_i^l\right) - \Gamma_{th}\right)^2 + \left(\Gamma_h\left(f_i^u\right) - \Gamma_{th}\right)^2 \qquad (1)$$

where Γ_v and Γ_h are the reflection coefficients in decibels for the vertical and horizontal polarization, respectively, Γ_{th} is a threshold value set to -25 dB, f_i^l and f_i^u are different frequency points at the lower and upper frequency band, respectively, and N is the number of frequency points at each frequency band. It should be notice that each of the sums in (1) correspond to one of the aforementioned subproblems: OMT with PMW analyzed at the lower frequency band and OMT with PEW analyzed at the upper frequency band.

The final dimensions of the optimized OMT are shown in Fig. 4. In Fig. 5, the electrical response of the OMT for both polarizations is presented. The stringent specifications of 25-dB return loss are fulfilled in both frequency bands. The simplicity of the final OMT geometry that can be implemented by a total of six equal-thickness single-etch depth metal layers should be emphasized, as depicted in Fig. 1(c).

B. Layered Waveguide Bends

In order to get a proper interfacing with standard waveguides, it was decided to implement the flanges on the top and bottom of the metal layers, as shown in Fig. 7. In that way, the uniform and flat surfaces of the micromachined layers ensure a good alignment and electrical contact between the micromachined OMT and the external waveguides [22]. To this end, layered waveguide bends compatible with the number and thickness of the OMT layers should be designed. In addition, the same orientation of the rectangular waveguides at the axial and lateral ports is desired.

Modified 90° bends in the E- and H-plane are used at the lateral and axial ports, respectively. The 90° bend in the E-plane should be implemented with only two layers. Additional degrees of freedom are obtained by changing the width of the waveguide, as depicted in the inset of Fig. 6(b). The electrical response is optimized for at least 35-dB return loss in the upper frequency band. For the 90° bend in the H-plane, a total of six layers can be used, leading to a broadband response over the complete useful rectangular waveguide bandwidth. The final response and geometries of both layered 90° bends are shown in Fig. 6.

The distance between the OMT and bends was selected according to the diameter of the WR-10 waveguide standard flanges. This can be appreciated in Fig. 7. The full-wave response of the OMT with the layered bends at the axial and lateral ports is shown in Fig. 5. A return loss of 25 dB is obtained in both frequency bands due to the high performance of the designed layered 90° bends.

C. OMTs Back-to-Back

The last issue to be solved is the square waveguide interface. Since there are no standard square waveguides, an indirect measurement procedure is required. Different approaches are commonly used, which require the design of additional custom-made components, such as waveguide transitions [23], dual polarization matched loads [24], or even different reactive loads [25]. Another option is to use a different OMT with the same square waveguide to measure the OMT under test. If both OMTs are equal, this alternative reduces to a back-to-back configuration. In this alternative, two OMT should be implemented; however, this is not a problem for micromachining techniques and both devices can be fabricated over the same wafer at the same time. With the aim of easing the final measurement process, we opted for the back-to-back configuration.

The distance between both OMTs is set according to the flange dimensions. The final back-to-back configuration, with the main advantage of using standard WR-10 waveguides at the four input/output ports, is shown in Fig. 7. Using the back-to-back configuration, a diminution of 6 dB (worst case) in the return loss for both polarization can be estimated. This is translated into around 19-dB return loss for the presented design. The full-wave simulation of the two OMTs in the back-to-back configuration, showing the mentioned diminution, is observed in Fig. 5.

(a)

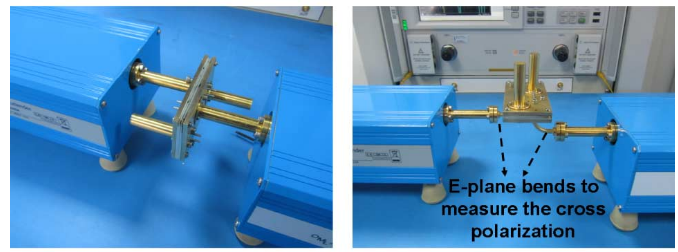

(b)

Fig. 8. (a) Photograph of the fabricated device. (b) Device in the measurement test set. In addition, two matched loads and two E-plane bends were used to measure all the scattering parameters of the four-port device.

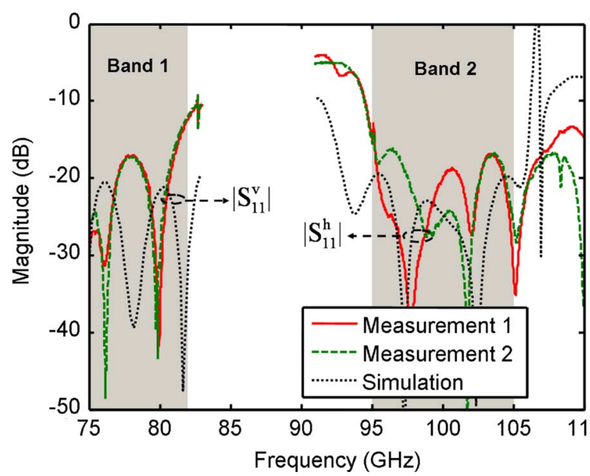

Fig. 9. Reflection coefficients measurements at both operating bands. Measurement 1 is $|S_{11}|$ and $|S_{22}|$ (see Fig. 7) at band 1 and 2, respectively. Measurement 2 is $|S_{33}|$ and $|S_{44}|$ (see Fig. 7) at band 1 and 2, respectively.

IV. Experimental Results

A. Fabrication Using a Micromachining Process Based on Thick SU-8 Photo-Resist Technology

The designed OMT was fabricated through an ultra-thick SU-8 photo-resist-based micromachining process. This process has been used before for the fabrication of different waveguide components [12], [14], [20]. First, SU-8 50 photo-resist was spin coated on a 100-mm silicon wafer and the edge bead was removed immediately. The wafer then rested on a leveled stage for few hours to allow the liquid resist to be self-planarized. After that, the wafer was baked at 65 °C and 95 °C subsequently and thereafter patterned using UV radiation through a mask. Post-exposure bake was conducted at 70 °C, which was relatively lower than the previous bake, to reduce the stress accumulating in the thick SU-8 layer. The pieces were developed in EC solvent and released from the silicon wafer using a KOH solution. Finally, the SU-8 pieces were metallized with silver in an evaporator.

For the present design, a total of three wafer runs were required, placing two layers per wafer. The two layers placed on the same wafer were selected as opposite and equidistant from the symmetry plane of the OMT, leading to wafers with: 1) first and sixth; 2) second and fifth; and 3) third and fourth layers, as enumerated in Fig. 7. In that way, possible variations in the SU-8 thickness between different wafers were partially compensated and the symmetry of the OMT was maintained. This is important in order to avoid the excitation of undesired modes and spurious resonances.

The complete circuit was assembled by stacking the six micromachined SU-8 layers and clamping between two brass plates, as illustrated in Fig. 7. These layers were carefully aligned by using four metallic pins with precise diameter, which also acted as the dowel pins to fit into the standard waveguide flange. A photograph of the assembled circuit is shown in Fig. 8(a).

B. Scattering Parameters Measurement and Discussion

The measurements of the scattering parameters of the OMTs in a back-to-back configuration were carried out using a PNA E8364C with two OML frequency extenders network analyzer and used thru-reflection-line (TRL) calibration. The two ports of the network analyzer were connected to two of the ports of the device, while the remaining ports were loaded with matched loads, as shown in Fig. 8(b). In that way, the four-port device is completely characterized by carrying out six different consecutive measurements with the network analyzer ports connected at: 1) ports 1 and 3; 2) ports 2 and 4; 3) ports 1 and 2; 4) ports 3 and 4; 5) ports 1 and 4; and 6) ports 2 and 3; following the numbering of Fig. 7. For the latter two measurements, additional bends should be used due to the size of the frequency extenders, as shown in Fig. 8(b). It should be highlighted that this routing allows an easy measurement of

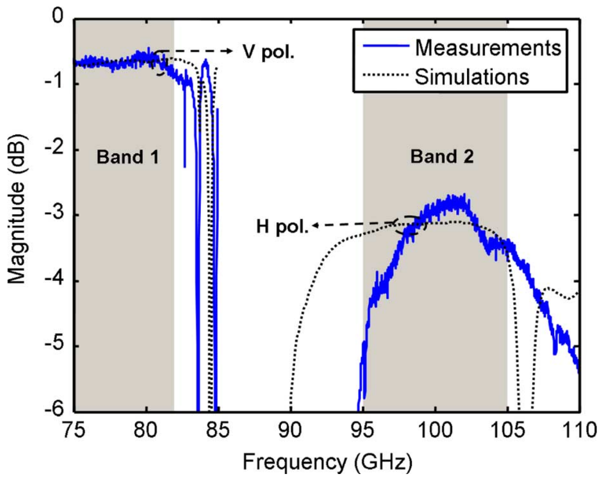

Fig. 10. Insertion loss measurements at both operating bands. The presented results correspond to the transmission measured between ports 1 and 3 at band 1 and between ports 2 and 4 at band 2 (see Fig. 7). An effective conductivity of $3 \cdot 10^6$ (S/m) and $1 \cdot 10^5$ (S/m) were use in the full-wave simulations for the vertical and horizontal polarization, respectively.

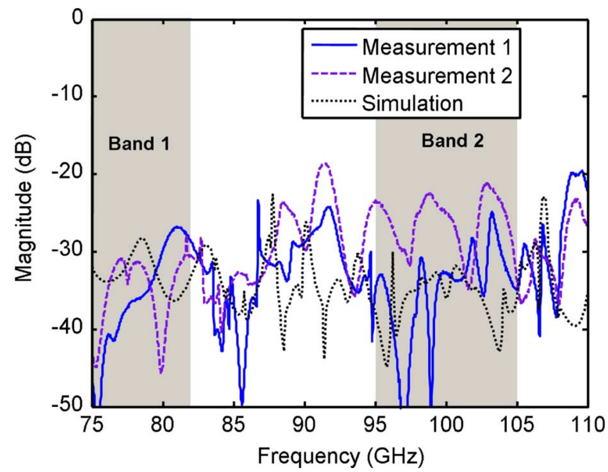

Fig. 11. Isolation measurements. Measurements 1 and 2 correspond to the transmission between ports 1 and 2 and between ports 3 and 4, respectively. The simulation was carried out assuming a misalignment of 10 μm at the symmetry plane of the OMT.

the circuit without rotating the frequency extenders and with the only additional components of two bends for the last two measurements.

In Fig. 9, the measurements of the reflection coefficient at both operating bands are presented. It can be appreciated around 16-dB return loss for both polarizations and certain frequency shift in the response. This frequency shift is associated with the fabrication tolerances of the micromachining process. The deviation of the measurements with respect to the simulations are of around 2 GHz to lower frequencies in the first band and around 2.5 GHz to higher frequencies in the second band. The discrepancies in the first band are mainly related to the tolerance in the thickness of the SU-8 layers. This is because the cutoff frequency of the vertical polarization is fixed by that dimension, as seen in Fig. 1(c). The 2-GHz frequency shift at the first band is equivalent to a layer thickness 4.5% larger than specified. On the other hand, the cutoff frequency of the horizontal polarization (band 2) is related with the patterned dimensions, as seen in Fig. 1(c). In this case, the 2.5-GHz frequency shift is equivalent to patterned dimensions 3% shorter than specified. These tolerance deviations of the micromachining process have been observed before in the microfabrication of different waveguide components [14], [18].

The measured insertion loss for both polarizations is shown in Fig. 10. An insertion loss of around 0.65 and 3.5 dB were obtained at the first and second bands, respectively. It can be noticed that these measurements correspond to signal paths going through both OMTs in the back-to-back configuration. The insertion loss of each of the single OMTs, including the long routing paths to the flanges and half of the square waveguide length, can be estimated as half of those values.

From the measured insertion loss, it is possible to define an effective conductivity. This value includes the effect of nonideal metallic conductors, surface roughness, air gaps, and any other possible issues during the fabrication [26]. Hence, the effective conductivity is highly dependent of the fabrication process and the nominal value of the metal conductivity might be considered as the upper limit. Moreover, for the case of double polarization devices, different insertion loss levels for each polarization are normally obtained [27]. This is because the electromagnetic field and particularly the surface current of each polarization is differently affected by the fabrication process. In that way, two effective conductivities, one per polarization, are required to characterize double polarization devices.

For the vertical polarization, an effective conductivity of $3 \cdot 10^6$ (S/m) was obtained, as shown in Fig. 10. It should be pointed out that this value is similar to the effective conductivity obtained at W-band using low-cost milling processes [28]. In the case of horizontal polarization, an effective conductivity of $1 \cdot 10^5$ (S/m) was obtained. This value is significantly lower than in the case of vertical polarization and can be due to air gaps in between micromachined layers. It is highlighted that the splitting of the device at the symmetry plane of the OMT interrupts the surface currents of the horizontal polarization. This fact explains the much lower effective conductivity achieved for this polarization. A possible solution for the air gaps issue might be a thermo bounding process once the circuit is assembled.

It is possible to observe some spikes out of band in Figs. 9 and 10. For the vertical polarization, the first spike above the first band is due to the cutoff frequency of the $\mathrm{TE}/\mathrm{TM}_{11}$ modes. This kind of spike has been observed before in dual-band OMT designs, such as in [3]. Above that frequency, the square waveguide is multimode and there are many resonances. For the horizontal polarization, there are a couple of spikes in the measurements above and below the second operating band. Out of the designed band, the OMT is not well matched and cavity resonances of the structure might probably appear.

The isolation, defined as the transmission between the rectangular waveguide ports, and the cross polarization isolation, defined as the transmission between a rectangular waveguide port and the orthogonal polarization at the common port, are ideally infinite due to the symmetry of the OMT. In practice,

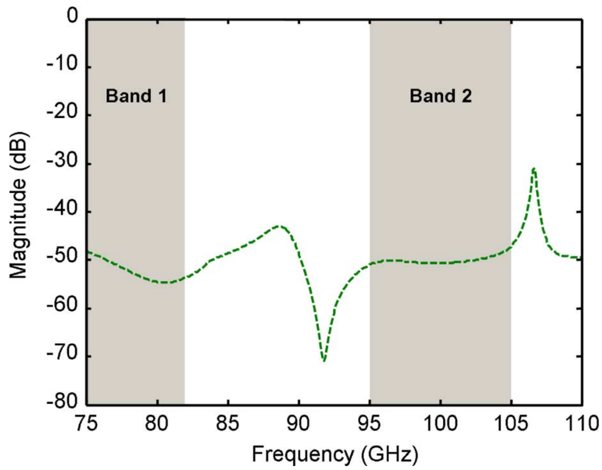

Fig. 12. Simulated isolation of a single OMT with a misalignment of 10 μm at the symmetry plane.

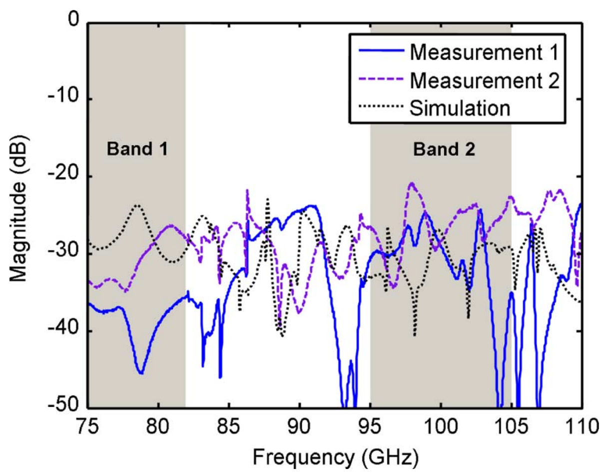

Fig. 13. Cross polarization isolation measurements. Measurements 1 and 2 correspond to the transmission between ports 1 and 4 and between ports 2 and 3, respectively. Additional external bends are included in the measurement (Fig. 8). The simulation was carried out assuming a misalignment of 10 μm at the symmetry plane of the OMT.

this symmetry is not perfect, leading to finite values of isolation and cross polarization isolation. The main cause for this loss of symmetry is the alignment precision between layers.

In Fig. 11, the measured isolations and the simulation of the back-to-back OMTs configuration are shown. The full-wave simulation was carried out introducing a misalignment of 10 μm at the symmetry plane of the OMT. The aim of this simulation is to get an estimation of the alignment accuracy of the device. From the data presented in Fig. 11, it is possible to estimate that the alignment precision is around 10 μm. It should be pointed out that the measured isolations shown in Fig. 11 are very pessimistic estimations of the isolation of a single OMT. This is due to the additional effect introduced by loading the common port of an OMT with an element (the second OMT) with cross polarization reflection coefficient $S_{11}\,(\mathrm{TE}_{10}, \mathrm{TE}_{01})$. Fig. 12 shows the full-wave simulation of a single OMT with a misalignment of 10 μm at the symmetry plane.

The measurements presented in Fig. 13 are mainly related to the cross polarization isolation of the OMTs. The simulation verify the previous estimation of around 10-μm precision in the layers alignment. In this case, the cross polarization isolation of a single OMT is fixed by the misalignment and the length of the square waveguide at the common port, as discussed in [8] and [29].

V. Conclusions

A new dual-band OMT with a simple geometry for optimum fabrication with micromachining techniques has been presented. The proposed design avoids critical elements commonly used in OMT devices such as septums, pins, or irises, and fulfills stringent specifications of more than 10% fractional bandwidth for each band and 30% separation between bands. Moreover, the geometry can be split into only six equal-thickness single-etch layers, and in that way facilitate the micromachinig implementation.

Two prototypes operating at W-band have been fabricated in a back-to-back configuration using an SU-8 photo-resist micromachining process. The measurements validate the design and prove to the authors' knowledge for the first time the microfabrication with SU-8 of an OMT.

In addition, the presented design is suitable to be scaled to higher frequency, as well as implemented with different micromachining processes based on staked metallized layers.

Acknowledgment

The authors wish to thank F. Tercero, Centro Astronomico de Yebes, Guadalajara, Spain, for his valuable help with the measurement of the OMT.

References

[1] J. Uher, J. Bornemann, and U. Rosenberg, *Waveguide Components for Antenna Feed Systems: Theory and CAD*. Norwood, MA, USA: Artech House, 1993.

[2] A. M. Bøifot, "Classification of ortho-mode transducers," *Eur. Trans. Telecommun.*, vol. 2, no. 5, pp. 503–510, 1991.

[3] J. M. Rebollar, J. Esteban, and J. D. Frutos, "A dual frequency OMT in the Ku band for TT&C applications," in *IEEE AP-S Int. Symp.*, Jun. 1998, vol. 4, pp. 2258–2261.

[4] G. Chattopadhyay, B. Philhour, J. E. Carlstrom, S. Church, A. Lange, and J. Zmuidzinas, "A 96-GHz ortho-mode transducer for the polatron," *IEEE Microw. Guided Wave Lett.*, vol. 8, no. 12, pp. 421–423, Dec. 1998.

[5] M. Ludovico, B. Piovano, G. Bertin, G. Zarba, L. Accatino, and M. Mongiardo, "CAD and optimization of compact ortho-mode transducers," *IEEE Trans. Microw. Theory Techn.*, vol. 47, no. 12, pp. 2479–2486, Dec. 1999.

[6] P. Sarasa, A. Baussois, and P. Regnier, "A compact single-horn C/X dual band and circular polarized Tx Rx antenna system," in *IEEE AP-S Int. Symp.*, 2004, vol. 3, pp. 3039–3042.

[7] J. A. Ruiz-Cruz, J. R. Montejo-Garai, and J. M. Rebollar, "Optimal configurations for integrated antenna feeders with linear dual-polarisation and multiple frequency bands," *IET Microw., Antennas, Propag.*, vol. 5, no. 8, pp. 1016–1022, Jun. 2011.

[8] A. Dunning, S. Srikanth, and A. R. Kerr, "A simple orthomode transducer for centimeter to submillimeter wavelengths," in *Proc. 20th Int. Space Terahertz Technol. Symp.*, Charlottesville, VA, USA, 2009, pp. 191–194.

[9] O. A. Peverini, R. Tascone, G. Virone, A. Olivieri, and R. Orta, "Orthomode transducer for millimeter-wave correlation receivers," *IEEE Trans. Microw. Theory Techn.*, vol. 54, no. 5, pp. 2042–2049, May 2006.
[10] C. Armitage-Caplan *et al.*, "COrE (Cosmic Origins Explorer), A white paper," *arXiv:1102.2181* 2011.
[11] V. M. Lubecke, K. Mizuno, and G. M. Rebeiz, "Micromachining for terahertz applications," *IEEE Trans. Microw. Theory Techn.*, vol. 46, no. 11, pp. 1821–1831, Nov. 1998.
[12] M. J. Lancaster, J. Zhou, M. Ke, Y. Wang, and K. Jiang, "Design and high performance of a micromachined K-band rectangular coaxial cable," *IEEE Trans. Microw. Theory Techn.*, vol. 55, no. 7, pp. 1548–1553, Jul. 2007.
[13] C. H. Smith, III, H. Xu, and N. S. Barker, "Development of a multilayer SU-8 process for terahertz frequency waveguide blocks," in *IEEE MTT-S Int. Microw. Symp. Dig.*, 2005, pp. 1–4.
[14] C. A. Leal-Sevillano, J. R. Montejo-Garai, M. Ke, M. J. Lancaster, J. A. Ruiz-Cruz, and J. M. Rebollar, "A pseudo-elliptical response filter at W-band fabricated with thick SU-8 photo-resist technology," *IEEE Microw. Wireless Compon. Lett.*, vol. 22, no. 3, pp. 105–107, Mar. 2012.
[15] C. Jung-Kubiak, J. Gill, T. Reck, C. Lee, J. Siles, G. Chattopadhyay, R. Lin, K. Cooper, and I. Mehdi, "Silicon microfabrication technologies for THz applications," in *IEEE Silicon Nanoelectron. Workshop*, Jun. 2012, pp. 1–2.
[16] K. M. K. H. Leong, K. Hennig, C. Zhang, R. N. Elmadjian, Z. Zhou, B. S. Gorospe, P. P. Chang-Chien, V. Radisic, and W. R. Deal, "WR1.5 silicon micromachined waveguide components and active circuit integration methodology," *IEEE Trans. Microw. Theory Techn.*, vol. 60, no. 4, pp. 998–1005, Apr. 2012.
[17] J. R. Stanec and N. S. Barker, "Fabrication and integration of micromachined submillimeter-wave circuits," *IEEE Microw. Wireless Compon. Lett.*, vol. 21, no. 8, pp. 409–411, Aug. 2011.
[18] X. Shang, M. Ke, Y. Wang, and M. J. Lancaster, "Micromachined W-band waveguide and filter with two embedded H-plane bends," *IET Microw., Antennas, Propag.*, vol. 5, no. 3, pp. 334–339, 2011.
[19] Y. Li, P. Kirby, O. Offranc, and J. Papapolymerou, "Silicon micromachined W-band hybrid coupler and power divider using DRIE technique," *IEEE Microw. Wireless Compon. Lett.*, vol. 18, no. 1, pp. 22–24, Jan. 2008.
[20] Y. Wang, M. Ke, M. Lancaster, and J. Chen, "Micromachined 300-GHz SU-8-based slotted waveguide antenna," *IEEE Antennas Wireless Propag. Lett.*, vol. 10, pp. 573–576, 2011.
[21] W. H. Press, S. A. Teukolsky, W. T. Vetterling, and B. P. Flannery, *Numerical Recipes in Fortran*. Cambridge, U.K.: Cambridge Univ. Press, 1992.
[22] T. Skaik, Y. Wang, M. Ke, S. Qian, and M. Lancaster, "A micromachined WR-3 waveguide with embedded bends for direct flange connections," in *Eur. Microw. Conf.*, Sep. 2010, pp. 1225–1228.
[23] A. Navarrini and R. L. Plambeck, "A turnstile junction waveguide orthomode transducer," *IEEE Trans. Microw. Theory Techn.*, vol. 54, no. 1, pp. 272–277, Jan. 2006.
[24] G. Pisano, L. Pietranera, K. Isaak, L. Piccirillo, B. Johnson, B. Maffei, and S. Melhuish, "A broadband WR10 turnstile junction orthomode transducer," *IEEE Microw. Wireless Compon. Lett.*, vol. 17, no. 4, pp. 286–288, Apr. 2007.
[25] O. A. Peverini, R. Tascone, A. Olivieri, M. Baralis, R. Orta, and G. Virone, "A microwave measurement procedure for a full characterization of ortho-mode transducers," *IEEE Trans. Microw. Theory Techn.*, vol. 51, no. 4, pp. 1207–1213, Apr. 2003.
[26] F. J. Tischer, "Excess conduction losses at millimeter wavelengths," *IEEE Trans. Microw. Theory Techn.*, vol. MTT-24, no. 11, pp. 853–858, Nov. 1976.
[27] G. Bertin, B. Piovano, L. Accatino, and M. Mongiardo, "Full-wave design and optimization of circular waveguide polarizers with elliptical irises," *IEEE Trans. Microw. Theory Techn.*, vol. 50, no. 4, pp. 1077–1083, Apr. 2002.
[28] C. A. Leal-Sevillano, J. R. Montejo-Garai, J. A. Ruiz-Cruz, and J. M. Rebollar, "Low-loss elliptical response filter at 100 GHz," *IEEE Microw. Wireless Compon. Lett.*, vol. 22, no. 9, pp. 459–461, Sep. 2012.
[29] A. Navarrini, C. Groppi, and G. Chattopadhyay, "A waveguide orthomode transducer for 385–500 GHz," in *Proc. 21th Int. Space Terahertz Technol. Symp.*, 2010, pp. 23–25.

Carlos A. Leal-Sevillano (S'06) was born in Madrid, Spain, in 1986. He received the Telecommunications Engineer degree and Master degree in communications technologies and systems from the Universidad Politécnica de Madrid, Madrid, Spain, in 2009 and 2010, respectively, and is currently working toward the Ph.D. degree at the Universidad Politécnica de Madrid.

Since 2008, he has collaborated with the Grupo de Electromagnetismo Aplicado y Microondas, Universidad Politécnica de Madrid. During 2011, he was a visiting Ph.D. student with the School of Electronic, Electrical and Computer Engineering, The University of Birmingham, Edgbaston, Birmingham, U.K., and during 2012, with the NASA Jet Propulstion Laboratory (JPL), California Institute of Technology, Pasadena, CA, USA. He is currently a Part-Time Associate Professor with the Universidad Autónoma de Madrid, Madrid, Spain. His research interests include electromagnetic wave propagation in waveguide structures, analytic and numeric electromagnetic methods, passive devices in the microwave, millimeter-wave, and terahertz bands, and optimization techniques.

Yingtao Tian received the Ph.D. degree in mechanical engineering from Loughborough University, Loughborough, Leicestershire, U.K., in 2010.

After working as a Researcher with the Rutherford Appleton Laboratory, where he developed high-density interconnection for pixel detectors, he is currently focused on micro-fabrication of terahertz microwave circuits.

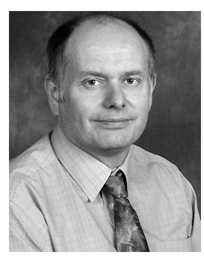

Michael J. Lancaster (M'91–SM'04) was born in Keighley, Yorkshire, U.K., in 1958. He received the Physics degree and Ph.D. degree from Bath University, Bath, U.K., in 1980 and 1984, respectively.

While with Bath University, he was involved with research into nonlinear underwater acoustics. After leaving Bath University, he joined the Surface Acoustic Wave (SAW) Group, Department of Engineering Science, Oxford University, as a Research Fellow, where his research concerned the design of new novel SAW devices including filters and filter banks. In 1987, he became a Lecturer with the Department of Electronic and Electrical Engineering, The University of Birmingham, Edgbaston, Birmingham, U.K., where he lectured on electromagnetic theory and microwave engineering. Shortly after he joined the department, he began the study of the science and applications of high-temperature superconductors, working mainly at microwave frequencies. In 2000, he became Head of the Emerging Device Technology Research Centre, and in 2003, Head of the Department of Electronic, Electrical and Computer Engineering. He has authored two books and over 170 papers in refereed journals. His current research interests include microwave filters and antennas, as well as the high-frequency properties and applications of a number of novel and diverse materials.

Prof. Lancaster is a Fellow of the Institution of Engineering and Technology (IET) and U.K. Institute of Physics. He is a Chartered Engineer and Chartered Physicist. He has served on the IEEE Microwave Theory and Techniques Society (IEEE MTT-S) International Microwave Symposium (IMS) Technical Committee.

Jorge A. Ruiz-Cruz (A'11–M'11–S'11) received the Ingeniero de Telecomunicación and Ph.D. degrees from the Universidad Politécnica de Madrid (UPM), Madrid, Spain, in 1999 and 2005, respectively.

Since 2006, he has been with the Universidad Autónoma de Madrid, Madrid, Spain, where in 2009, he became an Associate Professor. His current research interests are the computer-aided design of microwave passive devices and circuits (filters, multiplexers, ortho-modes, etc.).

José R. Montejo-Garai was born in Vitoria-Gasteiz, Spain, in 1965. He received the Ingeniero de Telecomunicación and Ph.D. degrees from the Universidad Politécnica de Madrid, Madrid, Spain, in 1990 and 1994, respectively.

Since 1989, he has been with the Grupo de Electromagnetismo Aplicado y Microondas, Universidad Politécnica de Madrid, as an Assistant Professor until 1996, when he became an Associate Professor. His research interests include the analysis and characterization of waveguide structures, advanced synthesis theory, and computer-aided design (CAD) for microwave and millimeter-wave passive devices: filters, multiplexers, OMTs, beam-forming networks, etc. He has designed several passive microwave devices for communication satellites.

Jesús M. Rebollar was born in Beasain (Gipuzkoa), Spain, in 1953. He received the Ingeniero de Telecomunicación and Doctor degrees from the Universidad Politécnica de Madrid, Madrid, Spain, in 1975 and 1980, respectively.

Since 1976, he has been with the Grupo de Electromagnetismo Aplicado y Microondas, Universidad Politécnica de Madrid, as an Assistant Professor until 1982, and an Associate Professor until 1988, after which he became a Professor of Teoría Electromagnética. His research interests include electromagnetic wave propagation in waveguide structures, interactions of electromagnetic fields with biological tissues, and particularly CAD for microwave and millimeter-wave passive devices: filters, multiplexers, polarizers, OMTs, beam-forming networks, etc. He has designed many of the above components for communication systems on board satellites.